A Generalized Transport Theory: Water-Mass Composition and Age

THOMAS W. N. HAINE

Earth and Planetary Sciences, The Johns Hopkins University, Baltimore, Maryland

TIMOTHY M. HALL

NASA Goddard Institute for Space Studies, New York, New York

(Manuscript received 31 March 2001, in final form 2 November 2001)

ABSTRACT

A general theory to describe and understand advective and diffusive ocean transport is reported. It allows any passive tracer field with an atmospheric source to be constructed by superposing sea surface contributions with a generalized Green's function called the boundary propagator of the passive tracer equation. The boundary propagator has the interpretation of the joint water-mass and transit-time distribution from the sea surface. The theory thus includes the classical oceanographic idea of water-mass analysis and extends it to allow for a distribution of transit times from the sea surface. The joint water-mass and transit-time distribution contains complete information about the transport processes in the flow. It captures this information in a more accessible way than using velocity and diffusivity fields, however, at least for the case of sequestration and transport of dissolved material by the ocean circulation. The boundary propagator is thus the natural quantity to consider when discussing both steady-state and transient ocean tracers, including the inverse problem of interpreting tracer data in terms of ocean circulation. Two constraints on the shape of the transit-time distributions are derived. First, the asymptotic behavior for a steady, or time-averaged, circulation is exponential decay. Second, integrated over the whole ocean, the transit-time distribution from the sea surface cannot increase. The theory is illustrated using a one-dimensional advection–diffusion model, a box model, and a North Atlantic general circulation model.

1. Introduction

Quantifying ocean transport is critical for understanding and better simulating climate change as the ocean is a dominant reservoir of heat, freshwater, and carbon. Direct observations of currents are, and likely always will be, too sparse in space and time to resolve unambiguously the important transport mechanisms. The most direct information on net transport is provided by the distribution of trace chemical species (tracers), both natural and anthropogenic. Tracers have the advantage that they reflect the total (advective plus diffusive) transport and that they capture integrated information about the circulation. There is a growing body of observations of tracers, such as the CFCs, ^{3}H, ^{3}He, ^{14}C (Schlosser et al. 1998). In contrast, there has not yet been a proportionate effort to interpret these data in terms of the ocean circulation. In part, this has been because the underlying theoretical framework has been lacking. Here, we propose a general theory for understanding ocean tracer fields and identifying the information they contain.

Corresponding author address: Dr. Thomas W. N. Haine, Dept. of Earth and Planetary Sciences, The Johns Hopkins University, 329 Olin Hall, Baltimore, MD 21218-2681.
E-mail: Thomas.Haine@jhu.edu

Determining the location of last surface contact and the mixing history of seawater, often referred to as water-mass analysis, is an oceanographic technique that has been in widespread use for nearly a century (Helland-Hansen 1916; Sverdrup et al. 1942; Wyrtki 1971; Worthington 1981; Tomczak 1999). For diffusive flow in a closed domain, after sufficient time, all regions are influenced by fluid that was at the boundary. The understanding of the structure of the global ocean in this way is an issue of fundamental importance in physical oceanography. With available instrumentation, there are just a few tens of characteristic water types that can be consistently distinguished over planetary distances and decadal timescales. In principle, water-mass analysis can be used to decompose an interior water parcel into fractions that originate from arbitrarily small regions of the sea surface, however.

The age of a water mass, the elapsed time since the water made last surface contact, is a concept that complements and extends water-mass analysis. Traditionally, oceanographers have relied on the semiquantitative interpretation of dissolved oxygen concentrations, judging the age by the oxygen deficit and (rather uncertain) respiration rates (Broecker and Peng 1982; Sverdrup et al. 1942). In the last 20 years the use of anthropogenic tracers with well-known time-varying tropospheric con-

centrations has permitted a more reliable estimate of timescales related to the water-mass age. The most important transient tracers in this class are the CFCs and ^{3}H and ^{3}He from atmospheric nuclear weapons tests (Bullister 1989; Jenkins and Smethie 1996). These man-made substances are inert in seawater and so are materially conserved following the flow [^{3}H decays to ^{3}He with a half-life of 12.4 yr (Taylor and Roether 1982)]. Measurements of these species can therefore be used to define various ''tracer ages'' based on the elapsed time since the value of some property derived from a tracer (or tracers) was last exhibited in the surface mixed layer (Doney and Bullister 1992; Haine and Richards 1995; Jenkins 1987). In typical practice, however, the tracer age deduced is different for each of these tracers (Haine et al. 1998; Doney and Jenkins 1988; Doney et al. 1997; England and Holloway 1998). It has been widely recognized that the tracer age only yields a good approximation of the water age in unrealistic circumstances, for example, when transport is dominated by simple bulk advection (Pickart et al. 1989; Haine et al. 1998). But it has been less appreciated how the various tracer-dependent ages are interrelated. Recently, there has been some recognition that the most appropriate way to discuss water-mass age is to consider a range (or distribution) of transit times from the water-mass formation regions [Beining and Roether 1996; Delhez et al. 1999; Khatiwala et al. 2001; Deleersnijder et al. 2001; see Hall and Plumb (1994) and Hall and Waugh (1997a) for the stratospheric case]. Nevertheless, the exact ways in which tracer ages are related to each other, to the water-mass age, and to the stirring and mixing in the ocean circulation have remained obscure.

Recent work on the transient-tracer inverse problem (Gray and Haine 2001) and atmospheric transport (Hall and Plumb 1994; Holzer and Hall 2000) provides a foundation to understand the relationships between water-mass composition, tracer ages, and the underlying transport processes in the flow. The key theoretical step is to recognize the importance of the Green's function of the tracer equation as the quantity that contains complete information about transport processes. Here, we exploit this theory to develop a conceptual and analytic framework for interpreting tracer distributions in terms of tracer-independent transport timescales and formation histories. The framework naturally includes the transit-time distribution and formation-region distribution (water-mass composition). In section 2 we review the concepts of water-mass composition and age. We then present the transport theory based on Green's functions and apply it to the oceanographic case (section 3). We illustrate these ideas using a simple analytical system, a box model, and then a water-mass–age analysis of a North Atlantic ocean general circulation model (section 4). The discussion of our theory and its implications are in section 5.

2. Background

Here we discuss the concepts of water-mass composition and age (section 2a) and review the ways ocean general circulation models have been tested with tracer observations (section 2b).

a. Water-mass composition and age

Quantitative water-mass analysis (sometimes called optimum multiparameter analysis) uses steady-state tracer observations to derive tracer-independent information about mixing in the ocean (Mackas et al. 1987; Tomczak and Large 1989; Wunsch 1996; Tomczak 1999). The method describes the composition of a water parcel in terms of the different fractions of component source waters. Mathematically, we express the tracer concentration as a linear combination of N source-water values. For example,

$$\theta = a_1\theta_1 + a_2\theta_2 + \cdots + a_N\theta_N$$
$$S = a_1S_1 + a_2S_2 + \cdots + a_NS_N \qquad (1)$$

for potential temperature θ and salinity S. Here a_i is the positive, dimensionless, fraction represented by the ith water-mass component. A water-mass component is defined by its geographic location at the time of permanent subduction from the mixed layer and S_i and θ_i are its tracer properties. The sum of all water-mass fractions is unity. Other steady-state tracers can be included in the analysis in the same way. The technique assumes the tracer properties are mixed conservatively in the ocean interior or have specified biogeochemical sinks (Poole and Tomczak 1999). It also requires different water masses to have distinct values of these tracer quantities (i.e., they carry independent information). These characteristics are set by diabatic air–sea interaction in the surface mixed layer. In practice, the individual water-mass fractions, a_i, are estimated from measurements of the various tracer properties of the water parcel using a nonnegative least squares method (Mackas et al. 1987). Typically, this decomposition into components yields fractions for a few ($N \approx 3$–6) broad categories of source waters. Poole and Tomczak (1999) provide a good example of this method with Atlantic thermocline data and attempt to include biogeochemical reactions and transient tracers.

In contrast to steady-state tracers, the primary and unique advantage of transient tracers is that they provide integrated information about transport timescales in the ocean. Interpretation of oceanic transient-tracer data has focused on the tracer age, which has been defined in various ways depending on the tracer in question. Perhaps the simplest tracer age is ''concentration age,'' namely, the elapsed time since the surface concentration was equal to the interior concentration. Concentration age is sensitive to both advection and mixing. It is often used for the CFCs (see, e.g., Doney and Bullister 1992). An alternative quantity is the CFC ventilation age (Wis-

egarver and Gammon 1988; Haine and Richards 1995). It depends on the differential behavior of two tracer species and is defined in terms of the concentration ratio of the two tracers; thus it is also referred to as a ''ratio age.'' The ratio age is the elapsed time since the surface ratio was equal to the interior ratio and has the advantage that it is unaltered by mixing with tracer-free water. Ratio ages are affected by mixing with tracer-labeled fluid, however (Pickart et al. 1989; Haine 1992). Radioactive tracers such as ^{3}H and ^{14}C carry an intrinsic isotopic clock. In this case, the tracer age is determined by the ratio of parent to daughter nuclide concentrations scaled by the appropriate half-life (Broecker and Peng 1982; Jenkins 1980). Again, this tracer age is sensitive to interior mixing (and, in addition, natural sources of ^{3}He and ^{14}C must be taken into account). Each of these tracer ages is significantly different from the water-mass age (Doney et al. 1997; England and Holloway 1998). While tracer ages have been put to good use for elucidating transport mechanisms, exploiting their information completely has not yet been possible. One reason is that the theoretical framework connecting tracers to *tracer-independent* transport information has been missing.

b. Ocean models and tracers

Recently, there has been a notable increase in the use of chemical tracers to assess ocean general circulation models [GCMs; England and Maier-Reimer (2001) provide a thorough review]. As tracer distributions reflect the total transport they are ideal for assessing subgrid-scale closure schemes in GCMs (Gent and McWilliams 1990; Visbeck et al. 1997). These studies confirm that the representation of the unresolved turbulent mixing processes has a crucial effect on GCM tracer fields. Another key process influencing GCM tracer distributions is the representation of the material exchange across the air–sea interface. Studies by Dixon et al. (1996) and England et al. (1994) using CFCs in coarse resolution global GCMs show oceanic uptake of these species is strongly affected by the uncertain parameterization of the air–sea tracer flux. The approach used in these studies has been to directly compare GCM tracer predictions with data. But tracers are sensitive to a variety of transport processes, and different tracers weight the processes differently. There have been few studies aimed at understanding GCM water-mass composition and age and evaluating GCM transport by exploiting tracers in combination. Such a description and approach is valuable, and one of our main aims is to provide a framework within which the complementary nature of different tracers is made apparent.

3. Tracer Green's function transport theory

Holzer and Hall (2000) and Gray and Haine (2001) have recently described passive tracer transport in the atmosphere and ocean using a Green's functions approach. Holzer and Hall (2000) also interpret the formalism in terms of transit-time distributions of fluid masses, generalizing the work of Hall and Plumb (1994). Green's functions are the conceptual tools at the heart of this theory to which we now turn.

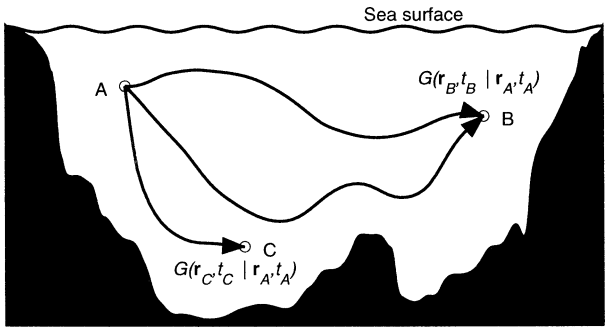

FIG. 1. Schematic of a Green's function component depicting the tracer concentration at the space–time positions *B* and *C* resulting from a source at the space–time position *A*. See section 3 for details. Modified from Gray and Haine (2001).

a. Tracer Green's functions and tracer age

The continuity equation for the concentration χ of a passive tracer is

$$\frac{\partial \chi(\mathbf{r}, t)}{\partial t} + L[\chi(\mathbf{r}, t)] = S(\mathbf{r}, t), \tag{2}$$

where L is a linear operator including, for example, advection and diffusive mixing due to unresolved eddies (or even molecular diffusion), and S is a tracer source or sink. Boundary conditions on the concentration, or the tracer flux, apply at the sea surface and seafloor.

The Green's function $G(\mathbf{r}, t \mid \mathbf{r}', t')$ is the solution to the related problem

$$\frac{\partial G}{\partial t} + L[G] = \delta(\mathbf{r} - \mathbf{r}')\delta(t - t'), \tag{3}$$

where δ is the Dirac delta function. Here G is the response of tracer concentration to an instantaneous impulse of tracer at time t' and position $\mathbf{r}'$ in the interior, including arbitrarily close to the boundary. This pulse of tracer spreads out into the ocean interior through the combined effects of advection and diffusion (Fig. 1). Considered as a function of $\mathbf{r}$, t, $\mathbf{r}'$, and t', G captures complete information about the transport processes in the flow.

The tracer field arising from a continuous source is a superposition of individual pulses,

$$\chi(\mathbf{r}, t) = \int d^3\mathbf{r}' \int_{t_0}^{t} dt' S(\mathbf{r}', t') G(\mathbf{r}, t \mid \mathbf{r}', t'). \tag{4}$$

Other inhomogeneous tracer sources are easily dealt with in a similar way (Gray and Haine 2001). It is pre-

cisely in the sense of (4) that tracer fields χ capture integrated information about the transport G.

The Green's function can be linked to the time since tracer was injected into the flow. The quantity $S(\mathbf{r}', t')G(\mathbf{r}, t \mid \mathbf{r}', t')/\chi(\mathbf{r}, t)$ is the fraction of tracer at $\mathbf{r}$ that has resided in the ocean an elapsed time $\tau = t - t'$ and thus represents a distribution of transit times τ since the tracer at $\mathbf{r}$ was injected. This distribution depends on the tracer source S, however. To obtain a distribution with a simple tracer-independent interpretation we are led to a related form of the Green's function sometimes called the ''propagator of boundary conditions.''

b. *Tracer boundary propagators and transit-time distributions*

Following Holzer and Hall (2000) we now consider the quantity $G(\mathbf{r}, t \mid \Omega, t')$, which satisfies the special case of (2) with no internal sources,

$$\frac{\partial G}{\partial t} + L[G] = 0. \tag{5}$$

The concentration boundary condition $G = \delta(t - t')$ is defined on a region Ω of the ocean surface (Ω typically covers the whole surface). No-flux boundary conditions apply elsewhere on the ocean surface and at the seafloor. Here G is called the propagator of boundary conditions on Ω (or simply the boundary propagator), such that, if on Ω there is a known time variation $\chi(\Omega, t)$, then in the interior

$$\chi(\mathbf{r}, t) = \int_{t_0}^{t} dt' \chi(\Omega, t') G(\mathbf{r}, t \mid \Omega, t'). \tag{6}$$

Although $\chi(\mathbf{r}, t)$ depends on the particular time variation of the boundary condition, G depends only on the fluid transport (advective and diffusive) from Ω to $\mathbf{r}$ (and on the geographic specification of Ω). Again, the boundary propagator contains complete information about the transport pathways and it can be directly connected to the Green's function G (Holzer and Hall 2000). There is an advantage in considering the boundary propagator, however. That is, it has the physical interpretation of the distribution of transit times since the fluid parcel at $\mathbf{r}$ had last contact with Ω (Hall and Plumb 1994; Holzer and Hall 2000). This can be seen by rewriting (6) using the transit time τ,

$$\chi(\mathbf{r}, t) = \int_{0}^{t-t_0} d\tau \chi(\Omega, t - \tau) G(\mathbf{r}, t \mid \Omega, t - \tau). \tag{7}$$

The boundary propagator acts to weight each transit time for every location $\mathbf{r}$ and time t. The concentration at every $\mathbf{r}$ and t consists of a sum of the boundary concentration multiplied by these weights. The boundary propagator G is thus a distribution function of transit times. It is sometimes called the age spectrum to reflect the spread of different transit times. Typically, we let t_0 extend into the distant past so the upper limit of the integral in (7) diverges. Now, it is easy to show that G is properly normalized by considering the case when $\chi(\Omega, t') = H(t - t')$, where H is the Heaviside function. After sufficient time, $\chi(\mathbf{r}, t)$ is arbitrarily close to one implying that

$$\int_{0}^{\infty} d\tau G(\mathbf{r}, t \mid \Omega, \tau) = 1 \tag{8}$$

as required. Beining and Roether (1996) also recognize that there is a range of transit times from the ocean surface to the interior rather than a single age. Nevertheless, they do not make the connection with Green's function theory or water-mass composition.

c. *Joint water-mass composition and transit-time distribution*

We now link the boundary propagator defined above and the water-mass composition and age ideas described in section 2a. To do so, we extend the definition of the boundary propagator to include multiple surface-source regions. The multiple-source boundary propagator, denoted G', satisfies the same equation as G,

$$\frac{\partial G'}{\partial t} + L[G'] = 0, \tag{9}$$

but is subject to different boundary conditions: $G' = \delta(t - t', \mathbf{r} - \mathbf{r}')$, where $\mathbf{r}'$ is on Ω, and no-flux conditions apply elsewhere. The interior tracer concentration can be built from G' in the usual way,

$$\chi(\mathbf{r}, t) = \int_{\Omega} d^2\mathbf{r}' \int_{t_0}^{t} dt' \chi(\mathbf{r}', t') G'(\mathbf{r}, t \mid \mathbf{r}', t'). \tag{10}$$

Comparing this expression to the analogous formula for the Green's function (4) highlights the important advantage of the boundary propagator. That is, using the boundary propagator we can construct the interior field by multiplying G' with the boundary concentration itself and integrating. Using the Green's function G we cannot obtain the interior field this way [see also Eq. (7) in Gray and Haine (2001)].

The implication of (10) is that G' can be interpreted as a joint water-mass composition and transit-time distribution. In particular,

- Of all the possible pathways from Ω to $(\mathbf{r}, t)$, $G'(\mathbf{r}, t \mid \mathbf{r}', t')\, dt' d^2\mathbf{r}'$ is the fraction of the water parcel at $(\mathbf{r}, t)$ that originated from the boundary region $d^2\mathbf{r}'$ in the time interval $t' \to t' + dt'$.

In other words, $G'(\mathbf{r}, t \mid \mathbf{r}', t')$ is a joint distribution function describing the water-mass composition at $\mathbf{r}$ and t as a simultaneous blend of waters from different surface-source regions and different times. This interpretation can be most easily understood by connecting a special case to the water-mass composition of section

2a. Consider a steady-state tracer whose surface concentration is piecewise constant over a series of N surface patches, $\Omega_1 \cdot \cdot \cdot \Omega_N$, of area A, which completely cover the sea surface. Using (10) we can write the interior concentration as

$$\frac{\chi(\mathbf{r}, t)}{A} = \chi(\Omega_1) \int_0^\infty d\tau G_1'(\mathbf{r}, \tau | \Omega_1) + \chi(\Omega_2) \int_0^\infty d\tau G_2'(\mathbf{r}, \tau | \Omega_2) + \cdots + \chi(\Omega_N) \int_0^\infty d\tau G_N'(\mathbf{r}, \tau | \Omega_N), \quad (11)$$

where we have assumed that the flow is stationary so that $G_i'(\mathbf{r}, t \mid \Omega_i, t') = G_i'(\mathbf{r}, t - t' \mid \Omega_i, 0)$. Comparison with (1) thus shows that the ith water-mass fraction is simply

$$a_i = A \int_0^\infty d\tau G_i'(\mathbf{r}, \tau | \Omega_i) \quad (12)$$

independent of any particular tracer, as expected. The multiple-source boundary propagator G' also allows for nonstationary flow, nonsteady tracer sources, and applies in the limit $N \to \infty$. It therefore generalizes the idea of water-mass composition to include a distribution of transit times for tracer originating from each surface-source point.

Note that G' is normalized in the sense that

$$\int_\Omega d^2\mathbf{r}' \int_{-\infty}^t dt' G'(\mathbf{r}, t | \mathbf{r}', t') = 1, \quad (13)$$

which follows by considering the case of $\chi(\mathbf{r}, t) = H(t - t')$. This normalization also implies the sum of the water-mass fractions is unity, as expected.

The multiple-source boundary propagator G' naturally extends the boundary propagator G. As they are related by $\int_\Omega d^2\mathbf{r}' G'(\mathbf{r}, t \mid \mathbf{r}', t') = G(\mathbf{r}, t \mid \Omega, t')$, $G'(\mathbf{r}, t \mid \mathbf{r}', t')d^2\mathbf{r}'$ is not itself a normalized distribution function of transit times since last contact with $d^2\mathbf{r}'$. Rather, it has the following interpretation: considering all the fluid at $\mathbf{r}$ and t to have originated from Ω at time t', $G'(\mathbf{r}, t \mid \mathbf{r}', t')d^2\mathbf{r}'$ is the transit time distribution for the fraction at $\mathbf{r}$ and t that touched $d^2\mathbf{r}'$. Contrast this case to a normalized transit-time distribution function with respect to $d^2\mathbf{r}'$ for a water parcel at $\mathbf{r}$. Such a distribution must account for the fluid that has been at the surface more than once (recirculated), passing through regions of Ω outside of $d^2\mathbf{r}'$. For such a boundary propagator, the recirculation dominates and, as $d^2\mathbf{r}' \to 0$, its first and higher moments diverge (Holzer and Hall 2000). On the other hand, for $G'(\mathbf{r}, t \mid \mathbf{r}', t')$ as we use it here, recirculated mass is not counted, but is rather removed by the zero-concentration condition everywhere on Ω outside $d^2\mathbf{r}'$. Other definitions are possible, but we advocate G' as the quantity that best represents the classical ideas of water-mass composition and age. Henceforth, we refer to G' simply as the boundary propagator.

d. Connection to tracer ages

Finally, we can make the connection to transient tracer ages. Consider a transient tracer age, CFC concentration age, for example. Following the ideas in section 2a, the concentration age is

$$\tau_{\text{conc}}(\mathbf{r}, t) = t - f[\chi(\mathbf{r}, t)], \quad (14)$$

where f is the inverse of the surface tracer-history function, namely,

$$f[\chi(\Omega, t)] = t \quad (15)$$

(Haine et al., 1998). (For the moment we restrict attention to the case where all the tracer comes from Ω—extension to multiple surface sources is straightforward.) Thus,

$$\tau_{\text{conc}}(\mathbf{r}, t) = t - f\left[\int_{-\infty}^t dt' \chi(\Omega, t') G(\mathbf{r}, t | \Omega, t')\right] \quad (16)$$

using (6). If the surface-tracer history is linear, then $\chi(\Omega, t') \propto t'$, and we find,

$$\tau_{\text{conc}}(\mathbf{r}, t) = \int_0^\infty d\tau \tau G(\mathbf{r}, t | \Omega, t - \tau) = \Gamma(\mathbf{r}, t). \quad (17)$$

In other words, the concentration age equals the mean transit time Γ. Note that the mean transit time is equivalent to the ideal age discussed by England (1995), for example. To see this, take the first moment of (5) to yield

$$\frac{\partial \Gamma}{\partial t} + L[\Gamma] = 1 \quad (18)$$

with the boundary condition $\Gamma = 0$ at the mixed layer. This expression is England's definition for ideal age (England 1995). Indeed, for steady transport, G is related to the transient ideal age Γ, the transient solution to (18), as $G = -\partial^2\Gamma/\partial t^2$ (Hall and Haine 2002).

If the surface-tracer history is not linear or still in a transient state, however, then (16) cannot be simplified. In this case, the concentration age depends on the details of the tracer source history. This circumstance generally applies, and similar arguments hold for ratio ages or ages from decaying radionuclides. So, transient tracer ages, like tracer concentrations, are convolutions of the boundary propagator (capturing tracer-independent information) and the transient-tracer history itself.

It is possible for tracer ages to be accurate estimates of the mean transit time if certain restrictive conditions about mixing apply (section 2a). The origin of these conditions can now be understood using the boundary propagator. Figure 2 shows forms of the transit-time distributions for which concentration age and ratio age

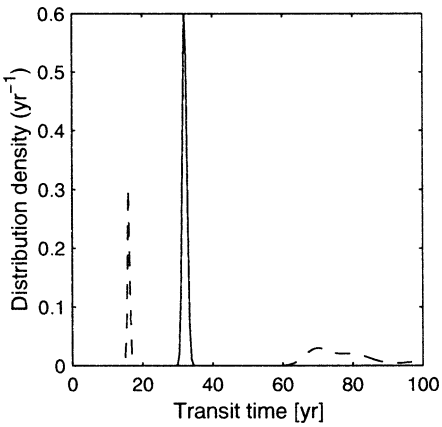

FIG. 2. Schematic transit-time distributions showing the functional forms required if CFC concentration age (full line), and CFC ratio age, or radioisotopic age (dashed line), accurately represent the true mean transit time. For the dashed line the shape of the transit-time distribution at transit times exceeding around 60 yr is unconstrained. The gap in transit times between the first and the second peaks must equal or exceed the timescale of the tracer transient itself. Currently, this timescale is about 60 yr for CFCs -11 and -12, and 45 yr for anthropogenic tritium.

give unbiased estimates of Γ. For concentration age, if the distribution is a delta function (no mixing at all), then the integral in the brackets of (16) can be evaluated to show that the concentration age equals the mean transit time. More generally, the tracer boundary condition need only vary linearly over the width of the transit-time distribution. For CFC ratio age and radioisotopic age we can tolerate mixing with old water if it is old enough to be free of tracer. Then the transit-time distribution is unconstrained for transit times longer than the timescale of the tracer transient itself. The boundary-propagator shapes in Fig. 2 are not typical, however, either in numerical models or in the real ocean. Therefore, concentration and ratio ages do not generally provide accurate estimates of the mean transit time. They still contain information about transport timescales, however, as we discuss in section 5.

4. Illustrative examples

We now present three examples to illustrate the boundary propagator approach to water-mass composition and age: a simple one-dimensional model, a box-mixing model, and a North Atlantic GCM.

a. One-dimensional idealized model

Perhaps the simplest nontrivial form of transit-time distribution, for a single tracer-source region, is a single peak with a long tail. Such a shape arises from the one-dimensional advection–diffusion problem in a semi-infinite domain. Indeed, this simple model has been commonly used to analyze and interpret ocean and atmospheric tracer measurements (e.g., Rehder et al. 1999; Hall and Waugh 1997b; Rhein 1994). We discuss the boundary propagator for this problem now.

In one dimension, the tracer continuity equation is

$$\frac{\partial \chi}{\partial t} + u\frac{\partial \chi}{\partial x} - k\frac{\partial^2 \chi}{\partial x^2} = 0, \tag{19}$$

where u is the velocity, k is the diffusivity, and the only tracer source is at $x = 0$. The boundary propagator, or transit-time distribution function, $G(x, t)$ is the response to a boundary condition $\delta(t)$ at $x = 0$. For constant, uniform u and k following standard methods yields

$$G(x, t) = \frac{x}{2\sqrt{\pi k t^3}} e^{-(ut-x)^2/4kt} \tag{20}$$

(Beining and Roether 1996; Hall and Plumb 1994). An alternative, and more useful, form is

$$G(t^*; \Gamma, \Delta) = \frac{\Gamma}{2\Delta\sqrt{\pi t^{*3}}} e^{-\Gamma^2(t^*-1)^2/4\Delta^2 t^*}, \tag{21}$$

where the nondimensional time is $t^* = t/\Gamma$. This distribution depends on the mean transit time Γ and width Δ (Δ^2 is half the variance of the distribution). These parameters are simply related to the current speed and diffusivity ($\Gamma = x/u$, $\Delta = \sqrt{kx}/u^{3/2}$). Equation (21) can also be used as a simple two-parameter distribution function without any explicit consideration of velocities and diffusivities (sometimes called the inverse Gaussian distribution).

The boundary propagator G is plotted in Fig. 3a at a point $x = 5000$ km downstream of the tracer injection site $x = 0$. Two cases are shown for typical values of u and k. For small k [small Δ and large Péclet number, $\text{Pe} = (\Gamma/\Delta)^2$], G is strongly peaked about the mean transit time Γ. The transport is nearly all advective, and the fluid mass is dominated by a single transit time. For larger k (moderate Δ and Péclet number), the fluid mass is comprised of elements having a wide distribution of transit times reflecting the diffusive transport pathways from 0 to x.

Figure 3b shows the concentration as a function of time for CFCs -11 and -113. The tracer concentration $\chi(x, t)$ is the average of the concentrations at the different transit times, and G represents the weighting of the average. The diffusive propagator gives higher concentrations because it preferentially samples younger fluid with higher concentrations. Although the diffusive propagator also has a tail extending to long transit times, older waters make a small contribution because they have weak concentrations. The CFC-11 surface concentration function is almost linear between the mid-1970s and 1990, and therefore the CFC-11 concentrations approach a value that reflects the mean transit time Γ [see (17) and recall that Γ is the same for both propagators]. For CFC-113 there is more curvature to the source history in these years and so it does not show the same convergence.

The corresponding concentration ages τ_{conc}, defined

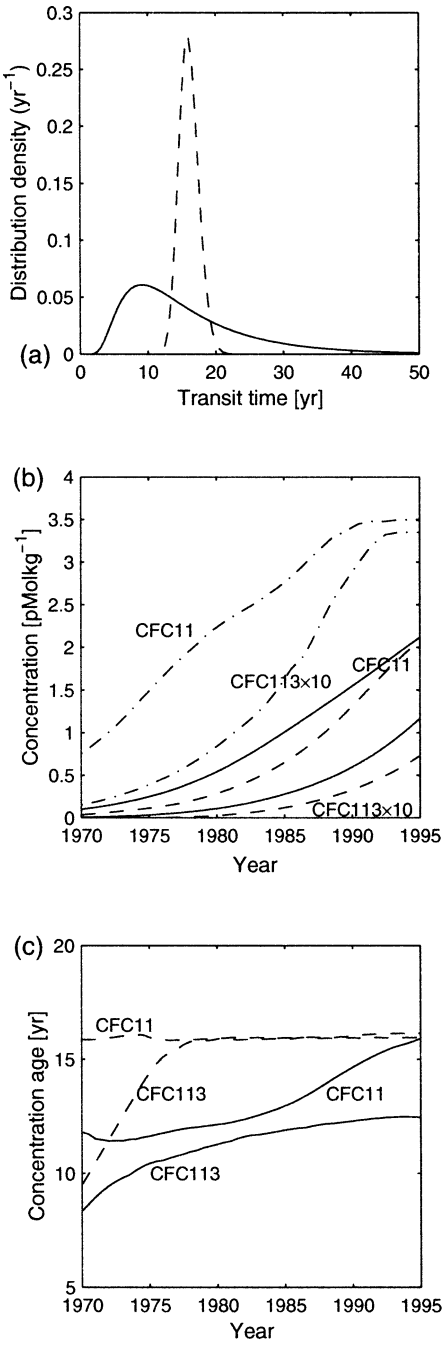

FIG. 3. Results of two cases from the illustrative one-dimensional advection–diffusion model (section 4a). The speed is 0.01 m s^{-1} for both examples and the diffusivity is 1×10^4 m^2 s^{-1} (full lines) and 2×10^2 m^2 s^{-1} (dashed lines). (a) Boundary propagators (yr^{-1}) 5000 km downstream from the source region. The corresponding mean transit times Γ and widths Δ are (16.1, 16.1)yr and (7.2, 1.0)yr for the full and dashed lines, respectively. The Péclet numbers are Pe = 5 and 250. (b) Evolution of CFC-11 and 10 × CFC-113 concentration (pMol kg^{-1}) at this site, for each propagator. We assume a constant temperature and salinity of 12°C and 35.00pss, respectively, and use the tropospheric source history of Walker et al. (2000) and solubilities of Warner and Weiss (1985) and Bu and Warner (1995). The saturated surface concentrations are shown with dash–dot lines. (c) Equivalent CFC concentration age (yr) for CFC-11, CFC-113, and each propagator.

by (16), are shown in Fig. 3c. For the advection-dominated propagator (dashed lines), there is good agreement between the CFC concentration ages and the mean transit time Γ, at least for the period since the CFCs have been varying. For the diffusive case, the concentration ages underestimate Γ because now there is a bias toward higher concentrations and hence younger fluid. The dilution with old (low CFC) water in the long-transit-time tail does not compensate sufficiently to correct this offset. The CFC-11 age approaches Γ in the 1990s because these waters mainly sample the period of linear CFC-11 increase, as explained above. In this idealized example, one could use the two concentration ages to constrain completely the transport, defined by Γ and Δ (or k and u), similar to the analysis of Hall and Waugh (1997b) in the stratosphere. In practice, while the functional form given by (21) captures certain features of more complex ocean models, it is not universal. We now turn to more general models of ocean transport: the box-mixing model and the North Atlantic GCM.

b. Box-mixing model

Box models of the ocean circulation have been extensively used to investigate transport of tracer constituents (see, e.g., Sarmiento 1983; Doney and Jenkins 1988; Wunsch 1988; Rhein 1994). Indeed, they are directly related to tracer models embedded in complex ocean GCMs. For both these reasons it is instructive to consider how our water-mass–age ideas apply in this context.

For convenience, we consider the box-mixing model of Fig. 4 as a crude representation of the zonally averaged meridional circulation in a midlatitude ocean basin. High-latitude surface waters sink and spread laterally to be returned to the surface at low latitudes and hence recirculated to the sinking region. There is tracer exchange with a tracer-laden atmosphere in the mid- and high latitudes (we imagine exchange with a shallow surface mixed layer whose tracer concentration is prescribed). The positive steady transport from the ith to the jth box is J_{ij}, which represents both advective (one-way) and diffusive (two-way) transport. The volume of each box is V, for simplicity, and thus the tracer concentration in the jth box evolves according to,

$$V\frac{dC_j}{dt} = \sum_i J_{ij}C_i - \sum_i J_{ji}C_j + F_j, \qquad (22)$$

where F_j represents the known boundary tracer source.

This linear system of coupled ordinary differential equations can be solved in the following way. Writing the 9×1 vector of tracer concentrations $\mathbf{C}$, we have

$$\frac{d\mathbf{C}}{dt} = \mathbf{AC} + \mathbf{BF}(t). \qquad (23)$$

Here the transport operator $\mathbf{A}$ is a 9×9 matrix containing the transports, $\mathbf{B}$ is a 9×9 diagonal matrix

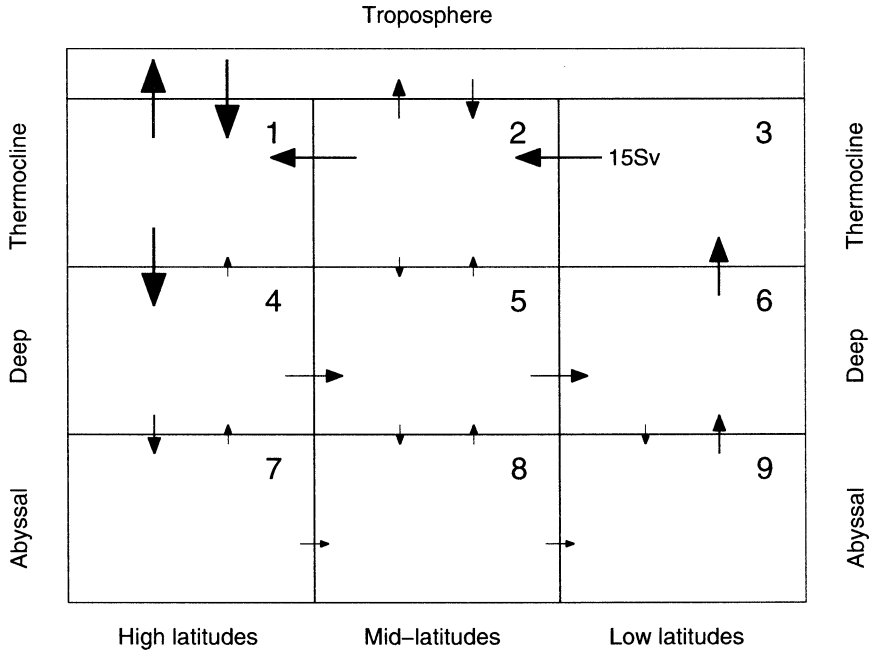

FIG. 4. Illustrative box-mixing model of the zonally averaged meridional overturning circulation in an ocean basin. Each box exchanges fluid with neighboring boxes according to the magnitude of the transport arrows shown. Boxes 1 and 2 are in contact with a surface mixed layer that sets tracer properties in the box model. For simplicity, each box has a volume of 10^{16} m^3 and the transports are steady.

specifying the boundary boxes (boxes 1 and 2 here), and **F** is the time-varying concentration boundary condition (only elements 1 and 2 of this vector are specified here). The solution to (23) is

$$\mathbf{C}(t) = e^{\mathbf{A}(t-t_0)}\mathbf{C}_0 + e^{\mathbf{A}t}\int_{t_0}^{t} e^{-\mathbf{A}t'}\mathbf{B}\mathbf{F}(t')\,dt', \quad (24)$$

where $\mathbf{C}_0$ is the initial condition at time t_0 (Boyce and DiPrima 1986). By analogy with (10), the boundary propagator, or joint water-mass–age distribution, is

$$G'_{ij}(\tau) = [e^{\mathbf{A}\tau}\mathbf{B}]_{ij}, \quad (25)$$

for transit time $\tau = t - t_0$ from the jth to the ith box. The Green's function is even more simple,

$$G_{ij}(\tau) = [e^{\mathbf{A}\tau}]_{ij}. \quad (26)$$

As expected, the joint water-mass–age distribution function depends only on the box-model transport (matrix **A**). For the example in Fig. 4, the joint water-mass–age distribution G'_{ij} is shown in Fig. 5.

There are several general remarks to make. Most important, the matrix exponential in (25) can be written using the eigen-decomposition of **A**,

$$G'_{ij}(\tau) = [\mathbf{V}e^{\lambda\tau}\mathbf{V}^{-1}\mathbf{B}]_{ij}, \quad (27)$$

where **V** is a matrix whose columns are eigenvectors of **A** and λ is a diagonal matrix of corresponding eigenvalues,

$$\mathbf{A}\mathbf{V} = \mathbf{V}\lambda. \quad (28)$$

The main advantage of this approach is to separate the time dependence explicitly. The boundary propagator can now be found without time integration of the box model; only eigen-decomposition of **A** is required. Direct integration over transit times can be performed to yield the water-mass decomposition,

$$a_{ij} = [\mathbf{V}(1/\lambda)\mathbf{V}^{-1}\mathbf{B}]_{ij}, \quad (29)$$

where a_{ij} is the fraction of the jth source at the ith box. These fractions are shown in Fig. 5 for the present example.

Transit-time moments from source j to box i are also easily found,

$$\frac{1}{a_{ij}}\int_0^\infty \tau^n G'_{ij}(\tau)\,d\tau = \frac{1}{a_{ij}}(n-1)!\left[\mathbf{V}\left(\frac{-1}{\lambda}\right)^{n+1}\mathbf{V}^{-1}\mathbf{B}\right]_{ij}, \quad (30)$$

for $n \geq 1$ (note the denominator normalizes the moments so they sum in the intuitive way, for example, $\Gamma_i = \Sigma_j a_{ij}\Gamma_{ij}$). In particular, the mean transit time from source j to box i, Γ_{ij} (first moment, $n = 1$), is shown in Fig. 5 for both surface source components. Next, note that the boundary propagator consists of superposed patterns with exponential time-dependence. There are nine transport timescales associated with the nine eigenvalues. Hence, we expect the long-term behavior of $G'_{ij}(\tau)$ to be exponential relaxation with a timescale given by the

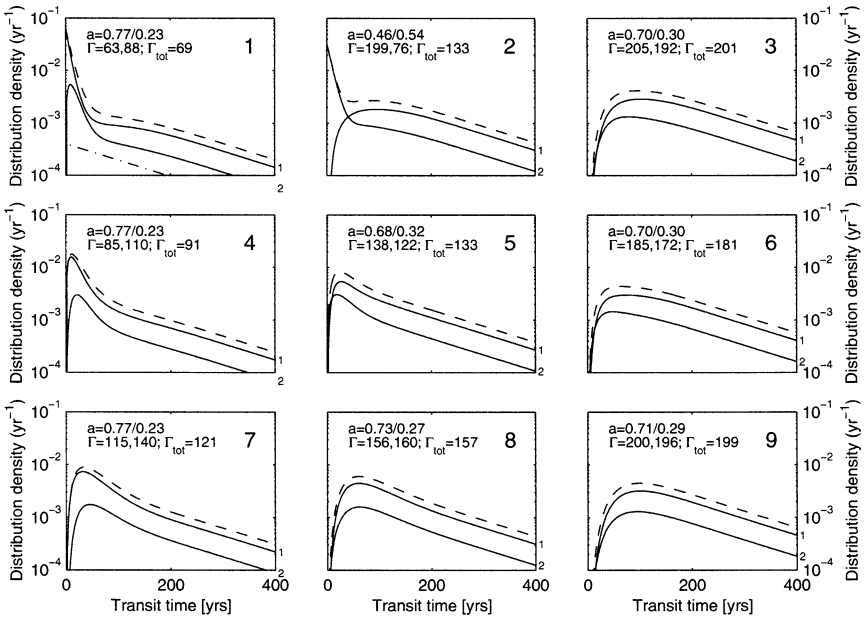

FIG. 5. Water-mass–age distribution [the transport propagator $G'_{ij}(\tau)$] for the box model of Fig. 4. Each panel shows the transit-time distribution of surface sources 1 and 2 (full lines), and the transit-time distribution from the whole surface (dashed line). The total water-mass fraction a and the mean transit time Γ (years) are shown for sources 1 and 2, respectively. Note the logarithmic scale for the propagator distribution. In box 1 the dot–dashed curve shows the decay of the eigenvector with smallest eigenvalue, which determines the long-term response.

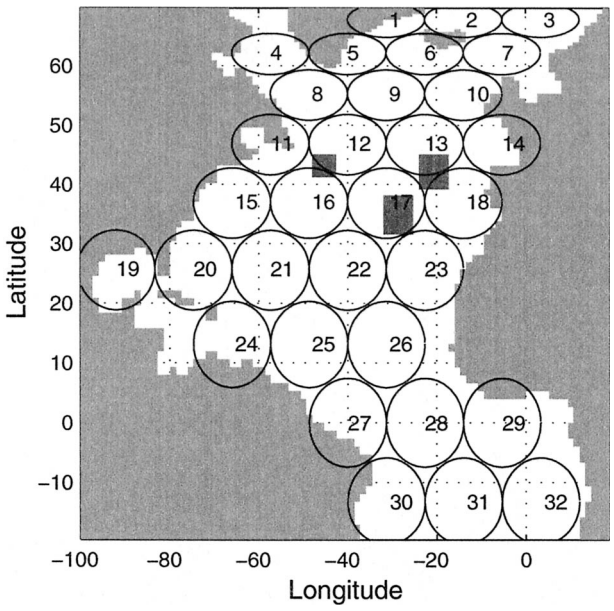

FIG. 6. Locations of 32 surface sources for the calculation of the MICOM boundary propagator. The ellipses show the contour of the Gaussian patch where the concentration has dropped to 1/e its peak value. The shaded boxes show the locations of the water-mass analysis sites in the eastern and central North Atlantic and at the Flemish Cap. These are shown in Figs. 8a, 8b, and 8c, respectively.

smallest eigenvalue, regardless of i of j. This curve is plotted in Fig. 5, box 1, and good agreement with the decay of the propagator tail can be seen. Also, by separating the time dependence in this way the interior tracer concentration for arbitrary boundary sources is reduced to a matrix product over the spatial dimension only. Finally, we emphasize that this argument applies generally to discretized circulation models; in principle, complex GCMs with steady transport can be treated in the same way (Wunsch 1988). Applying this method directly requires the eigen-decomposition of the transport operator but does not require separate integrations of the GCM. Extension of these ideas to nonsteady circulations is straightforward in principle although the time dependence is no longer separable as it is in (27) for the steady case.

c. General circulation model

We now use the Miami Isopycnic Coordinate Model to simulate the mean North Atlantic circulation on decadal timescales. The configuration is described by Gray and Haine (2001), so only a brief description is given here. The resolution is 4/3° in longitude and 4/3° × cos(latitude) in latitude, which yields an isotropic grid. There are sponge layers at the open boundaries (including the Straits of Gibraltar), 20 density layers in the vertical and a thermodynamically active mixed layer. The model is forced with monthly climatological fluxes derived from the ECMWF analysis (1986–1988) with

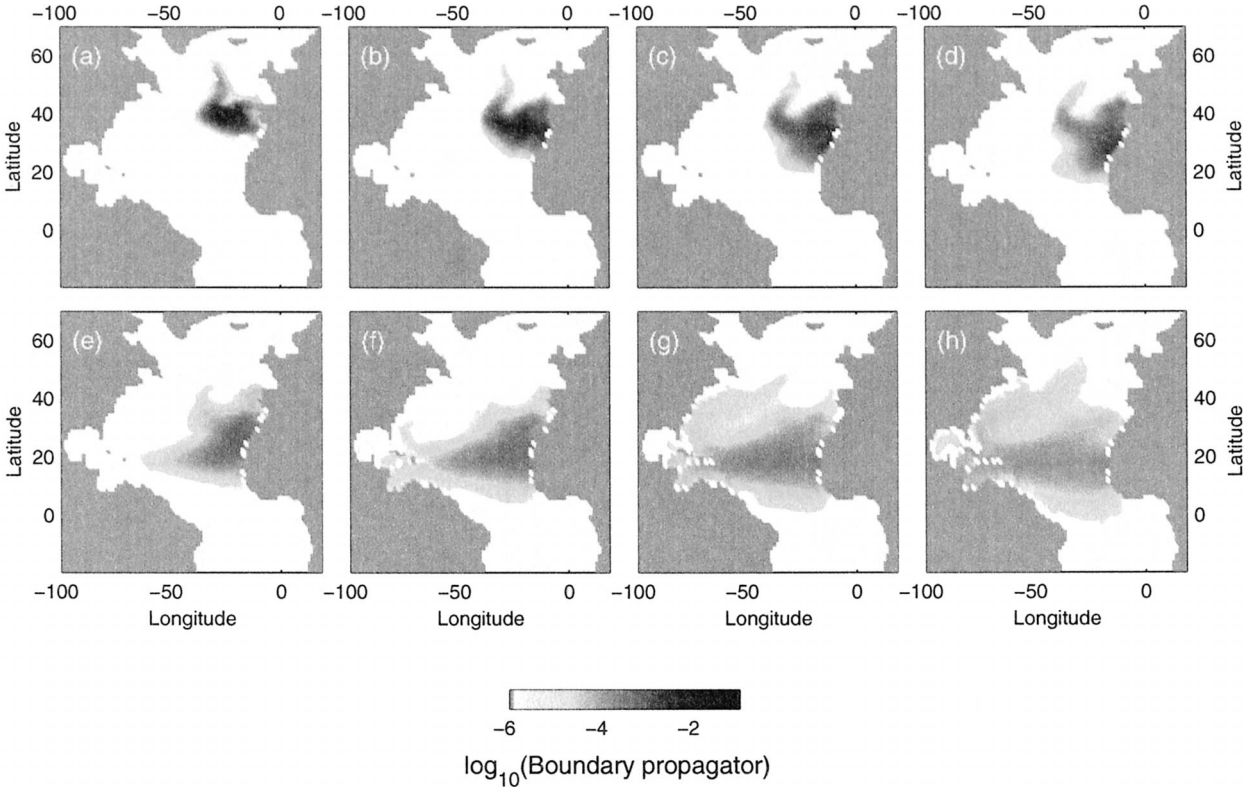

FIG. 7. Evolution of component 13 of the MICOM boundary propagator G' (logarithmic scale) on the σ_θ = 26.92–27.13 kg m^{-3} density layer. The propagator is shown at (a) 1, (b) 3, (c) 5, (d) 7, (e) 12, (f) 17, (g) 22, and (h) 27 yr after the tracer source. We show the layer-integrated propagator field because this quantity is conserved by the interior transport processes. As the boundary propagator is equivalent to the joint water-mass composition and transit-time distribution this diagram also has the following interpretation: The evolution of the boundary propagator at any given location is the transit-time distribution for the fraction of the water parcel that originates from surface patch 13 (see Fig. 6).

the sea surface salinity relaxing to the Levitus (1982) climatology. Subgrid-scale processes are parametrized using Laplacian diffusion along density surfaces with a small, realistic, diapycnal mixing. Our simulation begins from an adjusted flow, which is in steady state on annual timescales.

To derive the boundary propagator a tracer model is included in the dynamical code. The mixed layer tracer concentration is specified over 32 Gaussian elliptical patches for one month in February and March (Fig. 6). Thereafter, the mixed layer concentration is set to zero so as to simulate the boundary-propagator boundary condition. The tracer concentration for each tracer is then saved every 6 months for 200 yr. These concentration fields over space, time, and surface location comprise the discretized boundary propagator for the GCM. Although the GCM shows little interannual variability, there is a realistic seasonal cycle. In principle, therefore, we should repeat the 32 tracer releases several times during the year. In practice, doing so adds little information. The reason is that the interior ventilation process occurs for a short period in spring and the tracer patches do not spread out substantially over a few months (Gray and Haine 2001). The properties of the ocean interior are set by surface conditions at the end of winter (Williams et al. 1995). In contrast, the dominant interior transport timescales are a few years or decades.

Figure 7 shows the evolution of tracer ventilating the eastern North Atlantic on the σ_θ = 26.92–27.13 kg m^{-3} surface. As expected, we see tracer penetrating the gyre circulation as it follows the GCM transport pathways. Tracer is carried south and west round the subtropical gyre to join the rapid western boundary currents after 17 yr. The tracer is then spread back north along the model Gulf Stream and into the Southern Hemisphere through the North Equatorial Counter Current after 27 yr. A rapid route into the subpolar gyre also exists following the North Atlantic Current near the mid-Atlantic ridge.

The significance of the boundary propagator goes beyond a simple tracer of the flow because of its interpretation as the joint water-mass composition and transit-time distribution. The theory above shows that the boundary-propagator component in Fig. 7 can be interpreted as follows: For every geographic location, the boundary propagator time history is equivalent to the transit-time distribution for the fraction of water originating from the eastern North Atlantic in isopycnic layer σ_θ = 26.92–27.13 kg m^{-3}. Other surface locations

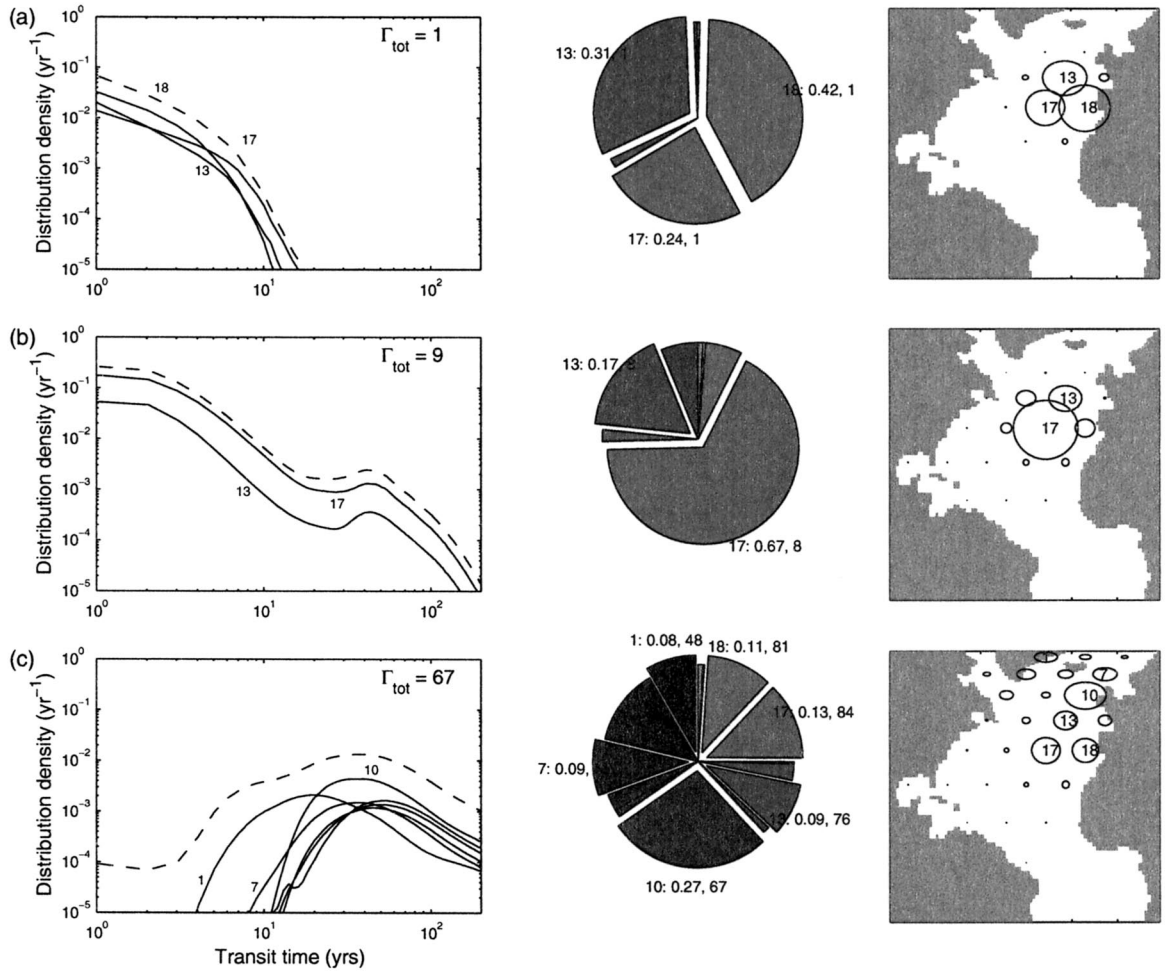

FIG. 8. MICOM water-mass composition–age distribution for (a) eastern North Atlantic mode water at 40°N, 20°W ($26.92 \leq \sigma_\theta \leq 27.13$ kg m^{-3}), (b) eastern North Atlantic mode water at 35°N, 30°W, (c) North Atlantic deep water at Flemish Cap 45°N, 50°W ($27.85 \leq \sigma_\theta \leq 27.90$), (d) subtropical mode water ($26.35 \leq \sigma_\theta \leq 26.92$), (e) subpolar mode water ($27.58 \leq \sigma_\theta \leq 27.85$), and (f) the whole model domain, excluding the mixed layer. In each case, the left panel shows the transit-time distributions for the important water sources (those that contribute 5% or more to the total composition estimated with transit times up to 200 yr). The transit-time distribution and the mean transit time (years) for all surface sources are shown with the dashed line and in the top right corner, respectively. The central panel shows the water-mass composition for all 32 sources shown in Fig. 6. The important sources are labeled with the source-location number, water-mass fraction, and mean transit time (years) for that source. Darker shades indicate northern sources. The right panel shows the locations of all sources with the area enclosed by the ellipse proportional to the water-mass fraction for that component. The important sources are labeled.

also ventilate this density horizon. To appreciate the relative importance of other sources, the joint water-mass composition and transit-time distribution is needed. This quantity is shown in Fig. 8 for six analysis sites. For each site, the transit-time distributions and water-mass compositions are shown for the most important surface sources (defined according to whether a source contributes 5% or more to the water mass). Also shown are the locations of these surface sources, their water-mass fraction, and mean transit time. For example, Fig. 8a shows that component 13 is 31% of the water mass on $\sigma_\theta = 26.92$–27.13 kg m^{-3} in the northeast Atlantic analysis box shown in Fig. 6 (centered near 40°N, 20°W at depths of around 250–350 m). The other significant sources are 17 and 18, which are also in the subtropical eastern Atlantic. The transit-time distributions for these sources are peaked at a transit time of 1–2 yr with a decay thereafter over a similar timescale. Waters with transit times of a few decades, or longer, are unimportant at this location.

Figure 8b shows a water-mass transit-time analysis at a site 1000-km downstream on the same isopycnic layer (near 35°N, 30°W and 400–600 m). Here, source 17 supplies two-thirds of the water. Now there is a second weak peak after about 50 yr corresponding to recirculation once about the subtropical gyre. This second peak cannot be accomodated by the one-dimensional boundary propagator functional form of section 4a. Figure 8c shows the sources of North Atlantic Deep Water (NADW) at Flemish Cap (45°N, 50°W, $27.58 \leq \sigma_\theta \leq 27.85$ kg m^{-3}, around

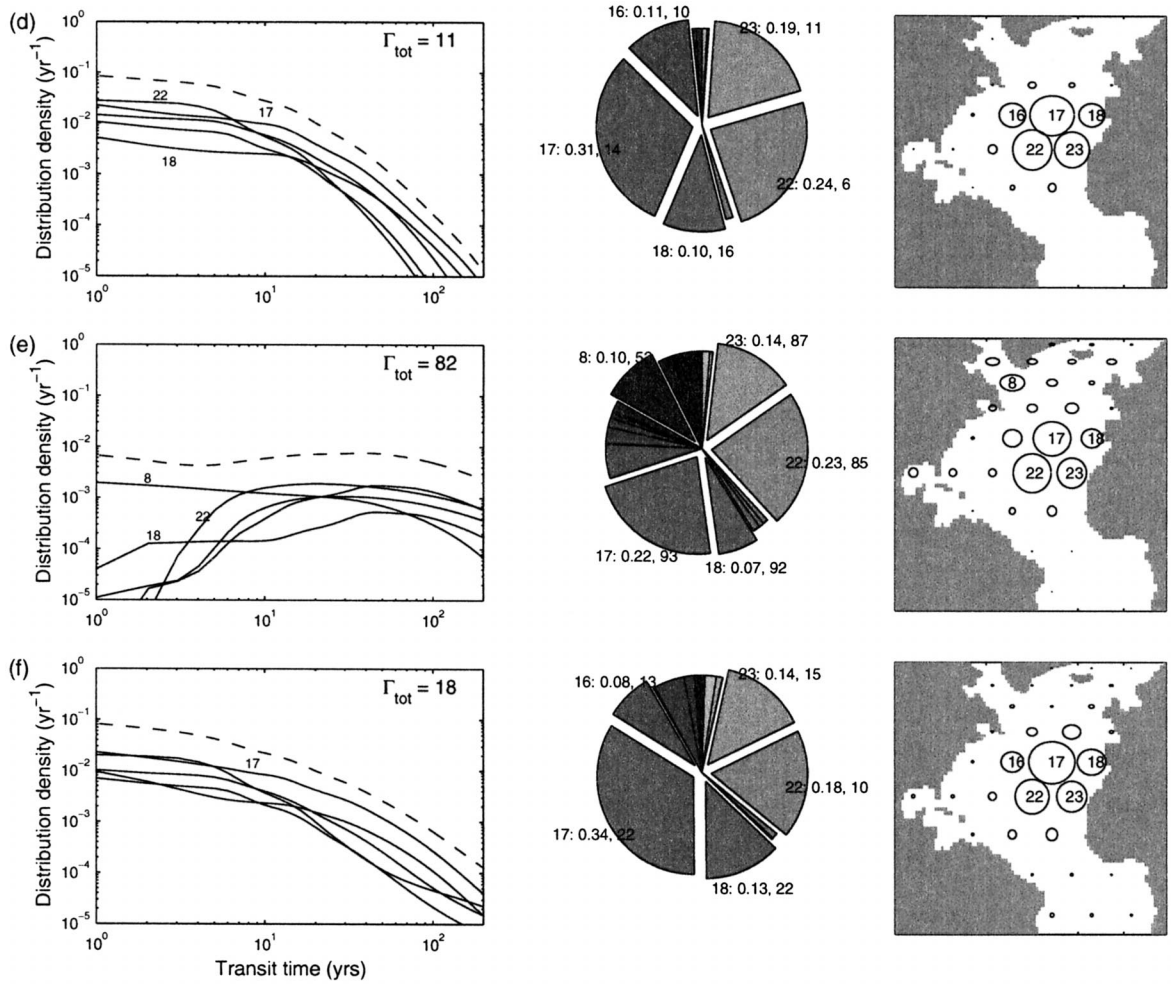

FIG. 8. (*Continued*)

3800-m depth). The youngest contributing waters come from source 1 in the Denmark Strait arriving with a modal time of about 18 yr. (There is also a weak local contribution from sources 8 and 12 at transit times of $O(1)$yr—it can be seen in the tail at short transit times in Fig. 8c.) Sources 7 and 10, in the Norwegian Sea and near Rockall, respectively, contribute next with peak transit times of a few decades. Interestingly, sources from the eastern Atlantic contribute about a third of the water overall (especially sources 13, 17, and 18) although they take around 50 yr to peak at this site. Of these significant sources, only sources 1 (Denmark Strait) and 7 (Norwegian Sea) have surface densities high enough to form NADW directly. Water from the other sources must therefore gain density through interior diabatic transformation. This conversion process presumably occurs in the subpolar gyre and by mixing with the Greenland–Scotland overflow waters, although the GCM may, of course, misrepresent it.

Figures 8d–f show the aggregated water-mass and transit-time composition of three large reservoirs in the North Atlantic GCM. In Fig. 8d we show the sources feeding subtropical mode water (STMW: σ_θ = 26.35–26.92 kg m^{-3}). The main sources for this water mass, which is one of the primary water types produced in the North Atlantic (Speer and Tziperman 1992), are in the central and eastern subtropics. Most STMW circulates round the subtropical gyre and is then entrained back into the mixed layer. Typical transit times are therefore a few years. There is little contribution from waters older than 10 or 20 yr. Figure 8e shows the sources of subpolar mode water (σ_θ = 27.58–27.85 kg m^{-3}), which is the second principal water type formed in the North Atlantic. Again the primary sources are in the eastern and central midlatitudes, although subpolar sources are more important. Apart from the Labrador Sea (source 8), which ventilates SPMW directly, most sources supply waters after transit times of a few decades via interior diapycnal fluxes. Finally, we consider the entire model domain as a whole (excluding the mixed layer).

Figure 8f shows that the same central and eastern subtropical sources dominate. As the most common transit times are a few years or decades, the mean total transit time for the whole domain is only 21 yr. This mean age underestimates the true value for two reasons: First, we have considered only waters with transit times less than 200 yr (the length of our integration). Some deep water masses are ventilated over longer timescales and they have been neglected. Second, by construction the GCM excludes old waters that enter the North Atlantic across the open boundaries. The mean transit time for the real North Atlantic Ocean is thus likely to be substantially larger due to the influence of dense Southern Hemisphere waters.

5. Discussion

In this article we present a general theory for understanding the distributions of passive tracers using a novel transport diagnostic: the joint water-mass and transit-time distribution, or boundary propagator. This quantity includes classical oceanographic water-mass analysis and extends it by allowing a range of transit times, or ages, from the ocean surface. It provides a theory for understanding both steady-state and transient ocean tracers using the same ideas. The joint distribution contains complete information about transport in the flow including advective and diffusive processes. It thus complements the traditional description of the circulation using current velocities and diffusivities. For some purposes, such as sequestration and dispersal of dissolved material in the ocean, it is more useful than the velocity and diffusivity fields themselves.

The joint water-mass and transit-time distribution is computed given a model of the ocean circulation. We illustrate this process using three examples of increasing complexity. Consideration of the simplest nontrivial boundary propagator shows why transient tracer ages provide biased estimates of the true mean transit time (section 4a). Analysis of the box-model example shows how the theory applies to systems that are discretized in space including the case of complex ocean GCMs. For steady (or time-averaged) circulations the propagator assumes an exponential decay at long transit times. In this case, it can be found by eigen-decomposition of the transport operator without resorting to direct integration. Such an approach can be applied to the transport solutions of hydrographic inverse calculations, for example. Using a coarse-resolution North Atlantic GCM we also demonstrate the interpretation of the boundary propagator as the joint water-mass composition and transit-time distribution. It provides valuable information about origin and timescales in the GCM circulation, which cannot be obtained directly from the velocity and diffusivity. We also identify diabatic transformation pathways in the GCM using the propagator.

The motive to interpret tracer data in the ocean is often to infer information about the circulation—the tracer inverse problem. The theory we present here illuminates this process. Referring to (10) we see that the inverse problem amounts to inverting the boundary-propagator convolution. That is, we wish to learn about G' given information about χ in the interior and at the ocean surface. In general, reversing such an integral transform is ill posed. The smoothing effect of integration means the data χ are insensitive to details of the propagator G'. Also, available ocean tracers sample only particular transit-time ranges. CFCs, for example, cannot be used to make inferences about transit times exceeding 60 or 70 yr. We can place some constraints on the shape of G' (for steady circulations the asymptotic behavior is exponential decay), but a wide range of behavior is still possible. Even in our coarse-resolution GCM there is great variety in the propagator time dependence (Fig. 8). While it has some basic similarities in shape to the the 1D advective–diffusive propagator often used to interpret field data (e.g., early peak followed by long tail), the GCM propagator exhibits features, such as multiple peaks that cannot be represented by such a simple functional form.

Despite these complexities, we believe that the natural quantity to estimate in the context of the tracer inverse problem is the boundary propagator. It reflects the transport processes in a more succinct way than the velocity and diffusivity fields. It also allows the information provided by observed tracers to be applied more directly to other trace constituents. (Note that if the goal is only to estimate an unknown tracer using other tracer data, accurate knowledge of the propagator may not be critical. The reason is the unknown tracer may be insensitive to the detailed propagator form making the task of inferring it from proxies easier than inferring the propagator itself.) A rational approach to interpreting tracer data, therefore, is to focus on the information that can be gleaned about the propagator, for example, by successive estimation of its moments. By posing the inverse problem in this way we can unambiguously identify the mutual and distinct information contained in both steady and transient tracer fields. The propagator is also the most useful quantity to discuss when comparing tracer dispersal in different model circulations. Only to the extent that the propagators are different, and that the tracers are able to probe these pathways, will two model tracer distributions differ. We advocate these approaches.

Perhaps the most important contribution here is that the joint water-mass and transit-time distribution is itself governed by the passive tracer equation. This result is not obvious and not trivial. It allows us to calculate this joint distribution in a straightforward way, at least for a GCM. It also has some important consequences. We close with a potentially powerful practical example: As the passive tracer equation [(2) with vanishing source S] conserves total tracer substance, so too is the volume-integrated boundary propagator conserved away from the sea surface. The inference is that, for any closed

volume, the volume-integrated propagator cannot increase with transit time. It can decrease, of course, by contact with the sea surface where the G' boundary condition is zero concentration. The volume-integrated transit-time distribution can, therefore, have only one peak at zero transit time. We also know that the propagator must decay exponentially with rate λ_{min} after a transit time of order $1/\lambda_{min}$ for steady, or time-averaged, circulation [λ_{min} is the smallest eigenvalue from decomposition of the transport operator (28)]. This restriction applies to the global ocean as a whole, for example, or the entire GCM domain (indeed, we see nonincreasing distributions for each water-mass component in Fig. 8f, as expected). This restriction on the time-dependence of the domain-integrated propagator greatly simplifies the tracer inverse problem, at least in principle, because estimates of only a few moments should be sufficient to allow a realistic reconstruction. It may also provide an important practical advantage in estimating the net air–sea exchange of atmospheric contaminants and the ocean's ability to absorb them. We are currently investigating the repercussions of this result for available tracers in the real ocean.

Acknowledgments. This study was supported by the National Science Foundation (OCE-9911318). Discussions with Suzanne Gray and Darryn Waugh were interesting and productive.

REFERENCES

Beining, P., and W. Roether, 1996: Temporal evolution of CFC 11 and CFC 12 concentrations in the ocean interior. *J. Geophys. Res.,* **101,** 16 455–16 464.

Boyce, W. E., and R. C. DiPrima, 1986: *Elementary Differential Equations and Boundary Value Problems.* John Wiley and Sons, 654 pp.

Broecker, W. S., and T. H. Peng, 1982: *Tracers in the Sea.* Lamont-Doherty Geological Observatory, Columbia University, 690 pp.

Bu, X., and M. J. Warner, 1995: Solubility of chlorofluorocarbons-113 in water and sea water. *Deep-Sea Res.,* **42A,** 1151–1161.

Bullister, J. L., 1989: Chlorofluorocarbons as time-dependent tracers in the ocean. *Oceanography,* **2,** 12–17.

Deleersnijder, E., J.-M. Campin, and E. J. M. Beckers, 2001: The concept of age in marine modelling. I. Theory and preliminary model results. *J. Mar. Syst.,* **28,** 229–267.

Delhez, E. J. M., J.-M. Campin, A. C. Hirst, and E. Deleersnijder, 1999: Toward a general theory of the age in ocean modelling. *Ocean Modelling,* **1,** 17–27.

Dixon, K. W., J. L. Bullister, R. H. Gammon, and R. J. Stouffer, 1996: Examining a coupled climate model using CFC-11 as an ocean tracer. *Geophys. Res. Lett.,* **23,** 1957–1960.

Doney, S. C., and W. J. Jenkins, 1988: The effect of boundary conditions on tracer estimates of thermocline ventilation rates. *J. Mar. Res.,* **46,** 947–965.

——, and J. L. Bullister, 1992: A chlorofluorocarbon section in the eastern North Atlantic. *Deep-Sea Res.,* **39A,** 1857–1883.

——, W. J., Jenkins, and J. L. Bullister, 1997: A comparison of ocean tracer dating techniques on a meridional section in the eastern North Atlantic. *Deep-Sea Res.,* **44A,** 603–626.

England, M. H., 1995: The age of water and ventilation timescales in a global ocean model. *J. Phys. Oceanogr.,* **25,** 2756–2777.

——, and G. Holloway, 1998: Simulations of CFC content and water mass age in the deep North Atlantic. *J. Geophys. Res.,* **103,** 15 885–15 901.

——, and E. Maier-Reimer, 2001: Using chemical tracers to assess ocean models. *Rev. Geophys.,* **39,** 29–70.

——, V. Garçon, and J.-F. Minster, 1994: Chlorofluorocarbon uptake in a World Ocean model. 1. Sensitivity to the surface gas forcing. *J. Geophys. Res.,* **99,** 25 215–25 233.

Gent, P. R., and J. C. McWilliams, 1990: Isopycnal mixing in ocean circulation models. *J. Phys. Oceanogr.,* **20,** 150–155.

Gray, S. L., and T. W. N. Haine, 2001: Constraining a North Atlantic Ocean general circulation model with chlorofluorocarbon observations. *J. Phys. Oceanogr.,* **31,** 1157–1181.

Haine, T. W. N., 1992: The use of transient tracers to study upper ocean processes. Ph.D. thesis, University of Southampton, 123 pp.

——, and K. J. Richards, 1995: The influence of the seasonal mixed layer on oceanic uptake of CFCs. *J. Geophys. Res.,* **100,** 10 727–10 744.

——, A. J. Watson, M. I. Liddicoat, and R. R. Dickson, 1998: The flow of Antarctic bottom water in the southwest Indian Ocean estimated using CFCs. *J. Geophys. Res.,* **103,** 27 637–27 653.

Hall, T. M., and R. A. Plumb, 1994: Age as a diagnostic of stratospheric transport. *J. Geophys. Res.,* **99,** 1059–1070.

——, and D. W. Waugh, 1997a: Timescales for the stratospheric circulation derived from tracers. *J. Geophys. Res.,* **102,** 8991–9001.

——, and ——, 1997b: Tracer transport in the tropical stratosphere due to vertical diffusion and horizontal mixing. *Geophys. Res. Lett.,* **24,** 1383–1386.

——, and T. W. N. Haine, 2002: On ocean transport diagnostics: The idealized age tracer and the age spectrum. *J. Phys. Oceanogr.,* **32,** 1987–1991.

Helland-Hansen, B., 1916: Nogen hydrografiske metoder. *Forhandlinger ved de 16 Skandinaviske Naturforsherermøte,* Vol. 39, Kristiania, 357–359.

Holzer, M., and Hall, T. M. 2000: Transit-time and tracer-age distributions in geophysical flows. *J. Atmos. Sci.,* **57,** 3539–3558.

Jenkins, W. J., 1980: Tritium and ^{3}He in the Sargasso Sea. *J. Mar. Res.,* **28,** 533–569.

——, 1987: ^{3}H and ^{3}He in the Beta Triangle: Observations of gyre ventilation and oxygen utilization rates. *J. Phys. Oceanogr.,* **17,** 763–783.

——, and W. M. Smethie, 1996: Transient tracers track ocean climate signals. *Oceanus,* **29,** 29–32.

Khatiwala, S., M. Visbeck, and P. Schlosser, 2001: Age tracers in an ocean GCM. *Deep-Sea Res.,* **48A,** 1423–1441.

Levitus, S., 1982: *Climatological Atlas of the World Ocean.* NOAA Prof. Paper 13, 173 pp. and 17 microfiche.

Mackas, D. L., K. L. Denman, and A. F. Bennett, 1987: Least squares multiple tracer analysis of water mass composition. *J. Geophys. Res.,* **92,** 2907–2918.

Pickart, R. S., N. G. Hogg, and W. M. Smethie, 1989: Determining the strength of the deep western boundary current using the chlorofluoromethane ratio. *J. Phys. Oceanogr.,* **19,** 940–951.

Poole, R., and M. Tomczak, 1999: Optimum multiparameter analysis of the water mass structure in the Atlantic Ocean thermocline. *Deep-Sea Res.,* **46A,** 1895–1921.

Rehder, G., R. S. Keir, and E. Suess, 1999: Methane in the northern Atlantic controlled by microbial oxidation and atmospheric history. *Geophys. Res. Lett.,* **26,** 587–590.

Rhein, M., 1994: The deep western boundary current: Tracers and velocities. *Deep-Sea Res.,* **41A,** 263–281.

Sarmiento, J. L., 1983: A tritium box model of the North Atlantic thermocline. *J. Phys. Oceanogr.,* **13,** 1269–1274.

Schlosser, P., W. M. Smethie, and J. R. Toggweiler, 1998: Introduction to special section: Maurice Ewing Sympoisum on Applications of Tracer Substance Measurements to Oceanographic Problems. *J. Geophys. Res.,* **103,** 15 815.

Speer, K., and E. Tziperman, 1992: Rates of water mass formation in the North Atlantic Ocean. *J. Phys. Oceanogr.,* **22,** 93–104.

Sverdrup, H. U., M. W. Johnson, and R. H. Fleming, 1942: *The*

Oceans: Their Physics, Chemistry and General Biology. Prentice-Hall, 1087 pp.

Taylor, C. B., and W. Roether, 1982: A uniform scale for reporting low-level tritium measurements in water. *Int. J. Appl. Radiat. Isot.,* **33,** 377–382.

Tomczak, M., 1999: Some historical, theoretical and applied aspects of quantitative water mass analysis. *J. Mar. Res.,* **57,** 275–303.

——, and D. G. B. Large, 1989: Optimum multiparameter analysis of mixing in the thermocline of the eastern Indian Ocean. *J. Geophys. Res.,* **94,** 16 141–16 149.

Visbeck, M., J. Marshall, T. Haine, and M. Spall, 1997: Specification of eddy transfer coefficients in coarse-resolution ocean circulation models. *J. Phys. Oceanogr.,* **27,** 381–402.

Walker, S. J., R. F. Weiss, and P. K. Salemeh, 2000: Reconstructed histories of the annual mean atmospheric mole fractions for the halocarbons CFC-11, CFC-12, CFC-113, and carbon tetrachloride. *J. Geophys. Res.,* **105,** 14 285–14 296.

Warner, M. J., and R. F. Weiss, 1985: Solubilities of chlorofluorocarbons 11 and 12 in water and sea water. *Deep-Sea Res.,* **32A,** 1485–1497.

Williams, R. G., M. A. Spall, and J. C. Marshall, 1995: Does Stommel's mixed layer ''demon'' work? *J. Phys. Oceanogr.,* **25,** 3089–3102.

Wisegarver, D. P., and R. H. Gammon, 1988: A new transient tracer: Measured vertical distribution of CCl_2FCClF_2 (F-113) in the North Pacific. *Geophys. Res. Lett.,* **15,** 188–191.

Worthington, L. V., 1981: The water masses of the World Ocean: Some results of a fine-scale census. *Evolution of Physical Oceanography,* B. A. Warren and C. Wunsch, Eds., The MIT Press, 42–69.

Wunsch, C., 1988: Transient tracers as a problem in control theory. *J. Geophys. Res.,* **93,** 8099–8110.

——, 1996: *The Ocean Circulation Inverse Problem*. 1st ed. Cambridge University Press, 442 pp.

Wyrtki, K., 1971: *Oceanographic Atlas of the International Indian Ocean Expedition*. National Science Foundation, 531 pp.